Supplementary Information Appendix

Previous models

A handful of theoretical models were developed to account for the non-dichotomous particle trajectories in DLD arrays (Table 1 in main text. Note that the table only considers stretched array designs and deterministic dynamics. Tilted square arrays are not within the scope of this paper). Diffusion could be a source for displacement angles between 0° and θ_p. Heller and Bruus proposed a model that included diffusion and particle size dispersion, which reproduced the continuous change in migration angle as a function of particle diameter [1]. They assumed that particles diffuse as they are advected by the flow in an array of point-like pillars. Heller and Bruus' theory, however, is not directly relevant to the deterministic dynamics studied in this paper.

Interestingly, non-diffusive dynamics can also give rise to particle trajectories that are neither zigzag nor bumping. Long *et al.* discovered another non-binary deterministic migration angle in the case where the row-shift (ϵ) is such that $MD_y = N\epsilon$ with M and N co-primes [2]. Long *et al.* called this non-binary behavior multi-directional sorting modes, and showed the existence of 3 or 4 different migration angles depending on M and N. In these models the pillars were treated as points, ignoring the flow distortion due to the finite pillar diameter (Figure 1C-F). Cerbelli also studied rational row-shifts in the case of pillars with finite size and also found multi-directional modes [3].

Kulrattanarak *et al* considered finite size pillar arrays with different geometric parameters D_x, D_y and N, and observed (numerically and experimentally) particle trajectories which they named "mixed motion", with angles in between zigzag and bumping modes [4]. According to the authors, mixed motion (which Kulrattanarak *et al* observed when $D_x/D_y \leq 2$) was associated with a symmetry breaking in the width of the two flow lanes at the two opposing pillars that define a gap. While this work provided a significant step forward in capturing the phenomenology of DLD with realistic geometries, it did not provide an explanation of how the symmetry breaking of the fluid lanes leads to mixed motion in specific geometries. Importantly, these authors considered the streamlines and separatrices as having the same symmetries as the pillar array, as proposed in the original theory.

Anisotropic permeability of a stretched DLD array

The problem studied in this paper is a pressure-gradient driven fluidic system in a perfectly periodic lattice of pillars. For these kinds of systems, several studies have shown that the micro-structure of the lattice can cause anisotropic permeability [4,5], where the flow direction is not aligned with pressure gradient direction. Therefore, small particles advected by the flow can follow trajectories with non-zero migration angle. When wall-bounded arrays are considered instead of an idealized infinite lattice,

the external walls impose additional boundary conditions. Some authors have assumed that the presence of the walls force the flow to have no lateral velocity (that is, zero average velocity perpendicular to the walls) in each unit cell, an assumption that results in the impossibility of anisotropic permeability [6]. However, recent experiments (included our own results in this paper) have shown that the dynamics of passively advected particles in wall-bounded stretched DLD arrays can exhibit a lateral velocity and therefore anisotropic permeability[7].

In the nanoDLD array considered in this paper, there are 125 pillars in between the walls delimiting a 50μm wide channel, and 1250 pillars in the axial direction between the inlet and outlet of the array. Whether the assumption that channel-bounding walls (which impose a global boundary condition) force a zero lateral velocity in each internal unit cell (a local flow pattern) is valid, or if the number of pillars within walls is large enough to be well approximated as an infinite array, can be addressed experimentally. Figure 4A of the main text show that small particles indeed have non-zero migration angle, consistent with the predictions of our model that assumes an infinite array. This agreement is then expected when the ratio of the width of the array (W) to the lateral pitch (D_y) is sufficiently large, that is, when $W/D_x >> 1$.

In the main text we studied the migration angle of particles in DLD arrays in terms of the local periodicity and pseudo-periodicity of individual particles in the Poincare recurrence map, resulting in what seemed to be an ergodic dynamics from an irrational rotation number map on a torus. To have a global representation of this dynamics, we calculated the angle between the axial direction and the average velocity field, and compared it to the migration angle calculated from the pseudo-periodicity. We define the average velocity as

$$\langle \vec{U} \rangle = \frac{1}{A} \int_A \vec{U}(\vec{r})\, dA$$

where $\vec{U}(\vec{r})$ is the velocity in position $\vec{r}$ of the unit cell and A is the area of the unit cell. The angle θ between the average velocity and the axial direction is

$$\theta = \tan^{-1}\left(\frac{\langle \vec{U} \rangle_y}{\langle \vec{U} \rangle_x}\right)$$

where $\langle \vec{U} \rangle_x$ and $\langle \vec{U} \rangle_y$ are the x-component and y-component of the average velocity $\langle \vec{U} \rangle$.

Figure S1 shows the dependence of the single trajectory based migration angle (Fig. S1A, same as Fig 4A in the manuscript) and the average velocity angle (Fig. S1B) on the ratio between pillar radius D_0 and the pitch distance D_y in y-direction. The two results, one using the recurrence map and individual trajectories, and the other computed using the velocity field directly, are remarkably close to each other. This suggests that the pseudo-periodicity described in the main text is a manifestation of the anisotropic permeability of the flow. Even when the average migration angle can be directly calculated from the average velocity in the unit cell, the Poincare recurrence map

introduced in our paper is essential to elucidate individual trajectories, and the structure of the flow lanes. In addition, the recurrence map allows us to calculate the finite-radius particle trajectories resulting from the interplay between the flow of individual particles and particle-pillar interaction.

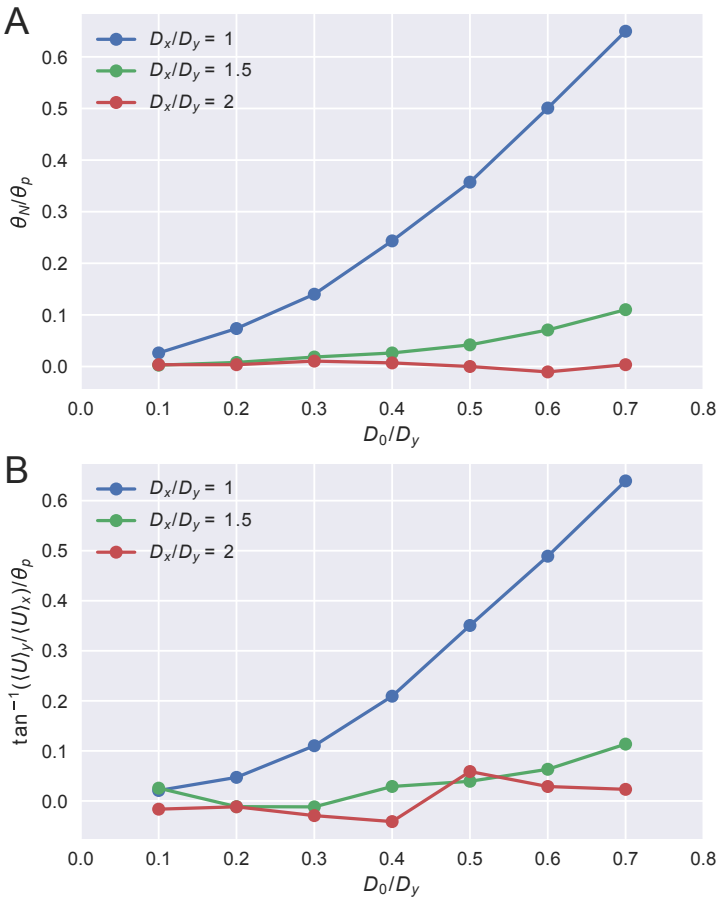

Figure S1 Normalized migration angle of particle trajectories and average flow velocity. (A) The migration angle obtained using the Poincare recurrence map and normalized by the pillar structural angle. θ_N is the migration angle calculated from a pseudo-periodicity N and θ_p is the structural pillar array angle determined by $tan^{-1}(\frac{D_y}{D_x N})$. (B) The angle of the average flow velocity in a unit cell normalized with the structural pillar array angle. D_x, D_y, D_0 are the pitch in x and y direction and the pillar diameter.

Recurrence map in a point-like pillar array

In general, the analytical form of the recurrence map f is unknown and needs to be computed using Stoke's equation with relatively complex boundary conditions. However, in the limiting case of negligible pillar diameter (point-like pillar system) the flow is not perturbed by the pillar array so that particles' trajectories are parallel to the x-axis of the array. In the recurrence-map coordinates, if a particle was at position $\eta_i(= y_i/D_y)$ at the inlet of the unit cell, the position of the particle $\eta_{i+1}(= y_{i+1}/D_y)$ at the next pillar inlet becomes $\eta_i - \epsilon/D_y$ because in the unit cell the y coordinates are measured with respect

to the bottom pillars, and the next pillar position has a y-axis shift by ϵ. (Note that in the main text we defined η as y/G but in a point-like pillar array $G = D_y$, and $\eta = y/D_y$.) Thus, in this case the recurrence map can be calculated analytically as following.

$$\eta_{i+1} = f(\eta_i) = \begin{cases} 1 + \eta_i - \epsilon/D_y & \text{if } \eta_i < \epsilon/D_y \\ \eta_i - \epsilon/D_y & \text{if } \eta_i > \epsilon/D_y \end{cases}$$

where we have used the unit cell periodic boundary conditions.

From the equation above we can calculate the local periodicity and the migration angle. Assume that the pillar array has a structural periodicity of N_p. This means that the array repeats its structure for translations of the form $x + N_p D_x$ in the x-direction. This symmetry requires that the row shift in the y-direction be $\epsilon = D_y/N_p$. We can calculate the sequence of positions measured at the inlet of the unit cell as the particle goes downstream. By iterating the recurrence map

$$f^{N_p}(\eta_0) = f\left(f^{N_p-1}(\eta_0)\right) = \eta_0 - N_p \frac{\epsilon}{D_y} = \eta_0 - 1 \equiv \eta_0$$

we see that the map returns to the original coordinate η_0 after N_p iterations. (At the last step in the previous sequence of iterations we used the periodic condition of map in the y-direction.) Therefore, the initial position η_0 is repeated over every N_p iterations. The sequence of these positions are:

$$\{\eta_0, \eta_1, \dots, \eta_{N_p-1}, \eta_0\}.$$

In this sequence, there are $N_p - 1$ direct transitions and one veering transitions. Because the flow periodicity and the pillar structural periodicity is same, the migration angle of small particle trajectories is zero. The lane dividing separatrices happen at inlet coordinates $\epsilon, 2\epsilon, \dots, (N_p - 1)\epsilon$. Particles starting at those points will end in stagnation points. Trajectories of particles within the flow lanes always have a periodicity of N_p.

We can also use the recurrence map to study multi-directional sorting modes[2]. For the case of $\epsilon = MD_y/N$ where M, N are co-primes, the recurrence map f is

$$f(\eta) = \begin{cases} \eta - \dfrac{M}{N} & \text{if } \eta > M/N \\ \eta - \dfrac{M}{N} + 1 & \text{if } \eta < M/N \end{cases}$$

With this recurrence map, we can calculate the N-th iteration position:

$$f^N(\eta) = \eta - M \equiv \eta.$$

In the last step, we use the periodic boundary conditions and the fact that M is an

integer number. Therefore, the initial position is repeated every N steps. However, in this case, the particle goes to the adjacent unit cell M times before it lands in the same original position η. Thus, the pseudo-periodicity in this case is N/M. Note that in this geometry, the symmetry of the streamlines still coincides with the symmetry of the pillar structure.

Local periodicity

The local periodicity of a long trajectory shows an intermittent behavior. Fig. S2 A – C shows several cycles in a long trajectory. Depending on the initial position, these cycles have local periodicities of any of two consecutive integer numbers N' and $N'+1$. The order in which N' or $N'+1$ occur is irregular. Still we can define the pseudo-periodicity by averaging over multiple local periodicities in a large trajectory. Thus, the average periodicity, which we call the pseudo-periodicity, is a non-integer number between N' and $N'+1$.

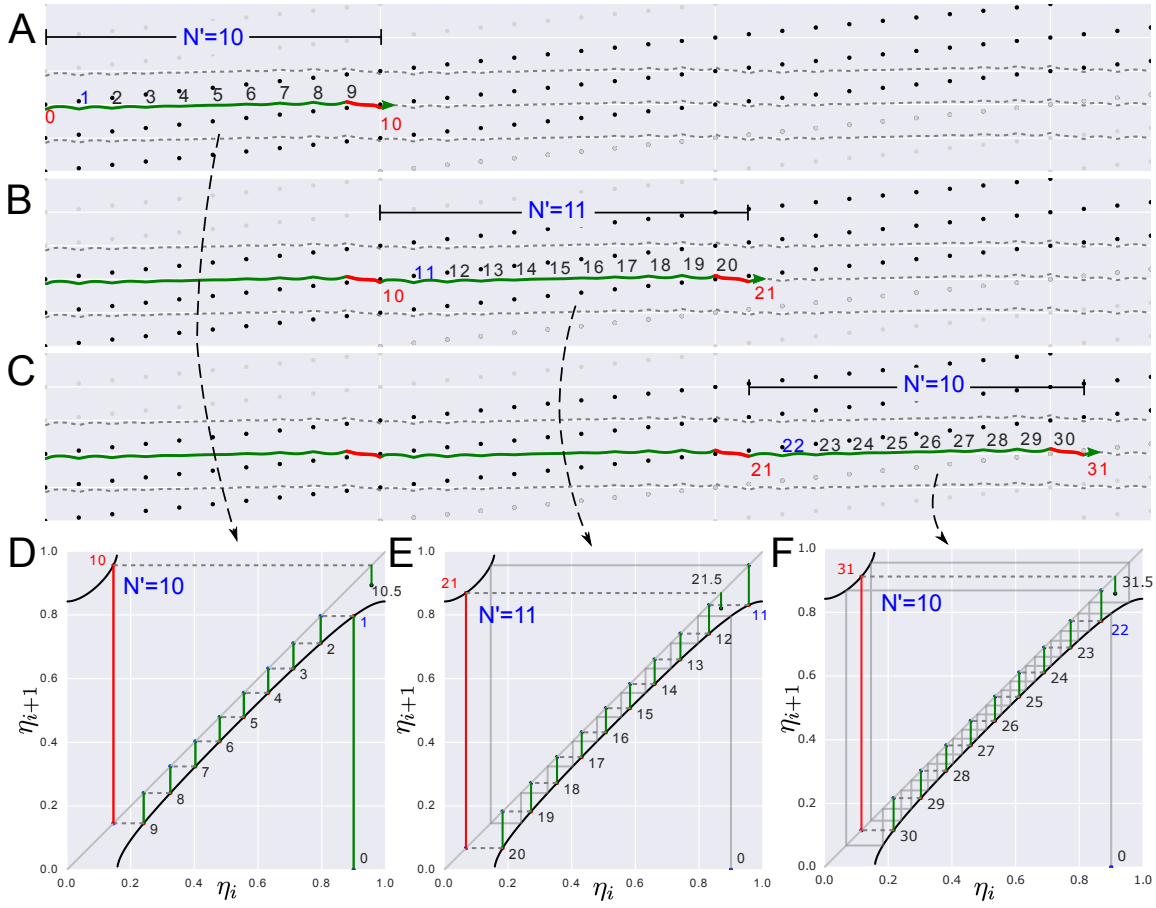

Figure S2. Long particle trajectory in a pillar array and the corresponding recurrence map. (A) The first cycle trajectory from one zigzag transition to next zigzag transition with local periodicity N'=10. (B) The second cycle trajectory with local periodicity N'=11. (C) The third cycle trajectory with local periodicity N'=10. (D) The recurrence map with N'=10 corresponding to the trajectory in (A). (E)The recurrence map with the next N'=11 particle positions overlaid with the previous cycle. (F) The recurrence map with

the next N'=10 particle positions overlaid with the previous two cycles. Here the pillar diameter is 40 nm and $D_x = D_y = 400$ nm. The row-shift distance is 40 nm so the structural periodicity N_p is 10.

Not every initial position at the inlet will have an infinite trajectory: some positions will, upon a finite number end up in the stagnation point at some pillar downstream. We call that set of points the stagnation set. To find the stagnation set, we first identify the inlet point $\eta_s$where the recurrence map is discontinuous ($f(\eta_s^-) = 1;\ f(\eta_s^+) = 0$). This is the starting point of the streamline that divides the veering streamlines ($\eta < \eta_s$) from the direct streamlines ($\eta > \eta_s$). The stagnation set can be computed by iteratively applying the inverse of the recurrence map f^{-1} to find all the points that the map to η_s.

$$\{\eta_0 = \eta_s \rightarrow\ \eta_{-1} = f^{-1}(\eta_0) \rightarrow\ \eta_{-2} = f^{-1}(\eta_{-1}\} \dots \rightarrow\ \eta_{-i-1} = f^{-1}(\eta_{-i}) \rightarrow \cdots\}$$

In general, this set is infinite. However, in the point-like pillar array, $\eta_s = \frac{\epsilon}{D_y} = \frac{1}{N}$, the above set is finite:

$$\{\frac{1}{N}, \frac{2}{N}, \dots, \frac{N-1}{N}, 1\}.$$

Note that the fluid flow brings the first position in this set, $\eta_0 = 1/N$, towards the stagnation point on the next pillar after one iteration. The point $\eta_{-1} = 2/N$ ends on the stagnation point after two iterations, and so on.

The pseudo-periodicity can be defined by the following formula:

$$\overline{N} = \lim_{L\to\infty} \frac{1}{L} \sum_{i=1}^{L} N_i'$$

where L is the number of cycles in a long trajectory and N_i' is local periodicity in the i-th cycle. In practice, the trajectory starts at some point η in the inlet of the unit cell. If is point belongs to the stagnation set, these iterations will eventually land on a stagnation point, and the computation of the pseudo-periodicity could proceed by iterating the map backwards. In any case, the stagnation set is countable (we can in principle count the pillars where the stagnation points will be) and therefore, this is a set of null measure. Therefore, with probability 1 the initial position η will not be in the stagnation set and we can find the next transition point infinitely.

Geometric dependence of the recurrence map

The recurrence map f is the mapping from the initial position at the inlet to the final position at the outlet. Therefore, as the streamlines veer differently depending on the geometry of the array, the recurrence map changes accordingly. Figure S2 shows the recurrence maps corresponding to different geometries, specifically differences in pillar

diameter. As the pillar diameter increases, the mapping f approaches the identity function $y = x$ and the local periodicity increases considerably. In this case the dynamics of the iterations resemble that of a dynamical system after undergoing a tangent bifurcation, which has been described as a route to intermittent chaotic behavior. In Fig. S2 the initial position was set at the middle of the gap and the map was iterated until the trajectories went through 400 cycles.

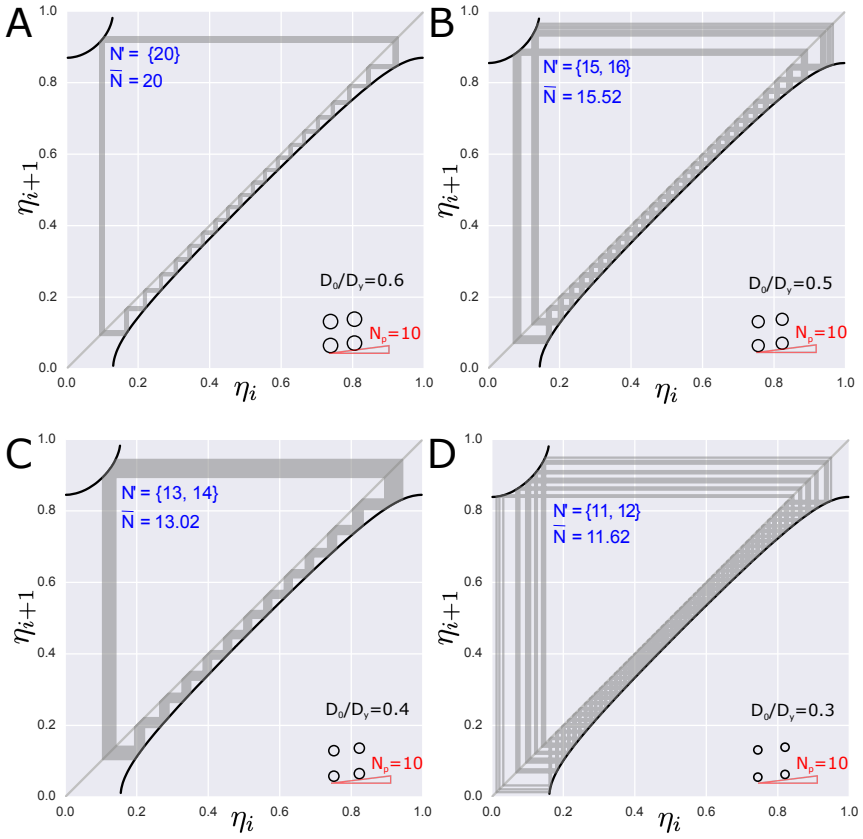

Figure S3. The recurrence map overlaid with multiple cycle positions in different geometries. (A)-(D) The pillar diameter D_0 is set to be 240, 200, 160, 120 nm, respectively. In all geometry, $D_x = D_y = 400$ nm and $N_p = 10$.

As the pillar diameter increases, the recurrence map approaches a tangent bifurcation due to two factors. One factor is the discontinuity points moves closer to the pillar surface, and the bundle of veering streamlines gets compressed. The second reason is that the curvature of a recurrence map near the discontinuity point increases, indicating that the streamlines close to the pillars are considerably perturbed. Thus, the ratio between the pillar diameter and the pillar to pillar distance strongly determines the shape of the recurrence map.

The transition cycles on the recurrence map has a rich variety of patterns. Fig. S3 shows two such patterns. One is the case in which the local periodicity persists but the final position of a cycle does not match the initial position of a cycle exactly, and there is a smooth drift of the subsequent cycles making the trajectories to form the band shown in Fig. S3 (A), (C). The other case is when the local periodicity oscillates between N' and

$N' + 1$. In this case the starting points of subsequent cycles may differ sufficiently that the local periodicity of subsequent cycles is different. Fig. S3 (B) and (D) shows that case in which the gray band in the recurrence map is more space filling than in the other two examples.

Reconstruction of trajectories

We derived a formula to connect the migration angle to the average streamline periodicity and the pillar structural periodicity.

$$\tan\theta = \frac{(\overline{N} - N_p)D_y}{\overline{N}N_p D_x}$$

where N_p is the pillar structural periodicity and $\overline{N}$ is the streamline periodicity. To confirm the calculation, we computed the particle trajectories over multiple pillar arrays using the calculated recurrence maps, as shown in Figure S4. The particle trajectories with three different initial positions are shown as green lines with zigzag type transitions in red. As discussed in the text, as the pillar diameter D_0 increases, the length of one cycle increases regardless of initial position (Fig. S4 A–D). Given the same initial positions, we can observe the migration angle increase as the pseudo-periodicity increases.

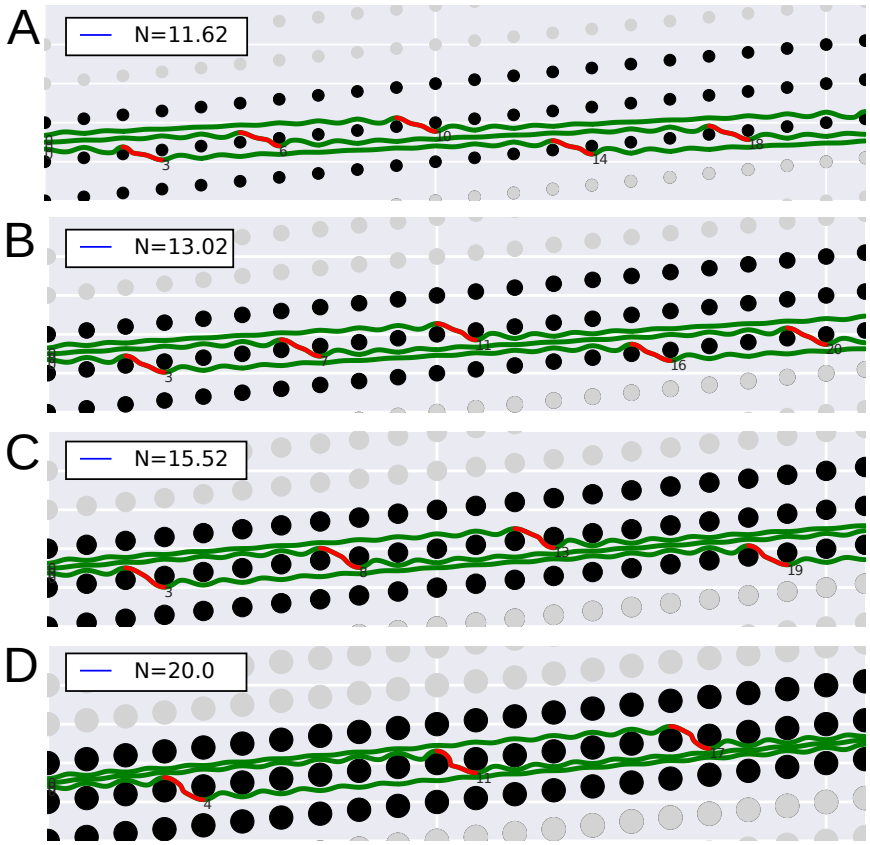

Figure S4. The reconstructed particle trajectory over multiple arrays (A)-(D). The pillar diameter is 120, 160, 200, 240 nm, respectively. The number located near a pillar indicates the index between two zigzag transitions (one cycle).

We can also check the lateral spreading from the three different trajectories. As the particles move, the lateral spread in the y-axis oscillates but then converges back to the original spacing after a single cycle. Therefore, in the deterministic case the pillars do not spread out the particle trajectory in the y-direction.

Initial position dependence on pseudo-periodicity

In a point-like pillar array, every trajectory is periodic and therefore all cycles have local periodicity N_p. In arrays with pillars of finite size, however, the pseudo-periodicity estimated as

$$\overline{N} = \frac{1}{L}\sum_{i=1}^{L} N_i'$$

of two trajectories starting at different initial positions are not always identical due to the finiteness of computation. Here, $L \gg 1$ is the number of cycles over a long trajectory.

Figure S5 shows a typical plot of the pseudo-periodicity as a function of the initial position of the long trajectory. We observed that most values are around the averaged

pseudo-periodicity ($\langle N \rangle = 10.81$) over all initial positions. The local periodicity alternates irregularly between 10 and 11. That the averaged periodicity $\langle N \rangle = 10.81$ means the local periodicity of 11 occurs more often than that of 10 over a long trajectory. In the experiments performed for this paper the particles were injected in the whole inlet of the array, and therefore the migration angle was estimated from the collective average over all individual trajectories. Therefore, our definition of averaged pseudo-periodicity is a reasonable choice to characterize the migration angle.

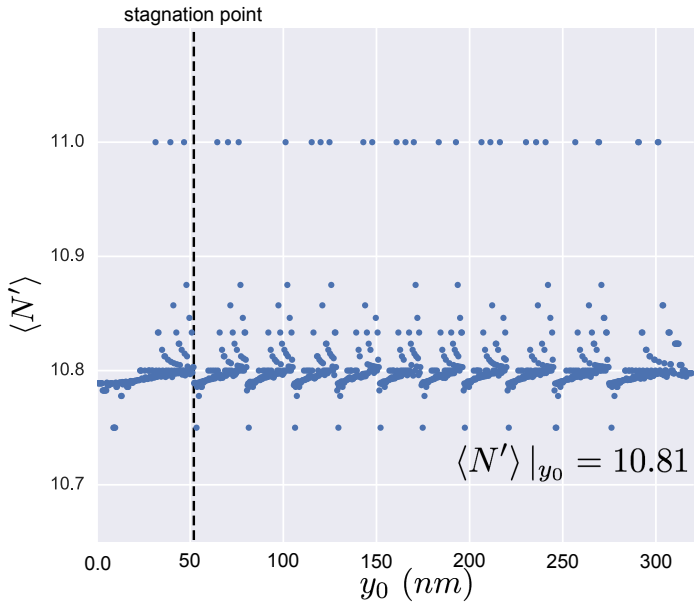

Figure S5. Pseudo-periodicity dependence on the initial position. Here, pillar diameter is 80nm and $D_x = D_y = 400$ nm. The pillar has a structural periodicity of $Np = 10$.

Recurrence map using 2 cells

Our simulations assumed a pillar array in a periodic lattice, which allowed us to solve the Stoke's equation in the unit cell. While this is a good approximation to model the actual system, this assumption may impose some limitations on the interpretation of the actual trajectories measured in finite size arrays in terms of our model. Here we will study two possible ways in which this approximation may influence our conclusions: one is the validity of our assumed pressure boundary conditions at the inlet and outlet of a unit cell, the other is the effect of the wall boundaries of the microchannel housing the pillar array on the particle trajectories. These two assumptions may be the cause of the differences between model and experiments seen in Figure 4 of the main.

The use of a single unit cell implies an infinite array in the x, y-directions. However, the pressure and velocity distributions of a multi cell array in which the boundary conditions are imposed at the input and output cells may be different from the pressure and velocity distributions if the boundary condition are imposed at the single unit cell. In our simulations, we applied a constant pressure on the inlet and outlet (AH, DE in Figure 1). To test that this is not too severe an approximation, we simulated several set

of combined unit cells (2x1, 2x2, 3x3 unit cells, still with periodic boundary conditions) to verify consistency with the 1x1 unit cell simulations. The resulting recurrence map showed no significant difference in either case.

The boundary conditions at the microchannel housing the pillar array may also have an impact on the fluid flow. In our experiments, the use of periodic boundary condition to mimic the infinite array can be justified by the fact that our nanoDLD device has 125x1250 unit cells inside the 50 μm wide microchannel. Thus, we can justify that our assumption of an infinite array is valid in the bulk of our arrays, as long as we are far from the boundaries. This is further justified by the observation that the experimentally measured migration angle matches well the one estimated with our model. To be more quantitative we simulated multiple arrays (15x20, 30x20, 45x20, 60x20 arrays) and observed that the effects of the walls started to be washed off at ~20 unit cells away from the microchannel boundary. The effect of the wall boundary conditions on particle trajectories in DLD arrays has also been discussed in [8].

Movie Description

The concept of the recurrence map can be more clearly understood using an animated description of the dynamics (Movie bump.mp4). Our animation shows the time evolution of a particle trajectory and connects it to the corresponding dynamics in a recurrence map. In the movie, the three panels from the left show the trajectory in multiple pillars, the trajectory in a unit cell and the recurrence map, respectively. Here, $N_p = 5$ and the pillar diameter D_0 is 200 nm. The pillar to pillar distance ($D_x = D_y$) is 400 nm so that the ratio (D_0/D_y) is 0.5. The long trajectory is composed of total 8 transition segments starting from 90% of the pillar gap ($\eta_0 = 0.9$).

For the particle with radius larger than the critical diameter (D_c), the trajectory is similar to that of the small particle until it veers around the pillar for the first time. But due to the shift of the center of particle by the pillar repulsion, it cannot veer around the pillar and bumps on the post surface. After it follows the closest possible streamline to the separatrix line, it ends up to the same initial position (the directional locking [9]). The animation in the middle shows this transition by overlaid trajectories inside a unit cell. In the recurrence map, the mapping f intersects the identity function ($y = x$) which becomes a fixed point in the dynamics. Here, blue circle means the initial position at the inlet and the red circle means the final position at the outlet.

Geometric parameters in the unit cell simulation

Four key parameters are used to specify the geometric configurations in our arrays, as shown in Fig. 1A: pillar diameter, D_0, the lattice parameters (pitch) of the pillar unit cell, D_x, D_y and the row shift fraction, ϵ. The value of these geometric parameters in the pillars used in this paper are summarized in the following Table S1.

Table S1 Geometric parameters in the unit cell simulation

	G (nm)	D_0 (nm)	D_x (nm)	D_y (nm)	N_p	D_0/D_y	Figure
1	380	40	400, 600, 800	400	10	0.1	2, 4
1	320	80	400, 600, 800	400	10	0.2	4, 5
2	280	120	400, 600, 800	400	10	0.3	1, 4, 5
3	240	160	400, 600, 800	400	10	0.4	1, 4, 5
4	200	200	400, 600, 800	400	10	0.5	1, 4, 5
5	160	240	400, 600, 800	400	10	0.6	1, 4, 5
6	120	280	400, 600, 800	400	10	0.7	4, 5

Here, we fixed the array structural periodicity as $N_p = 10$ and the pitch distance in y-direction at 400nm ($D_y = 400$ nm). Therefore, the only independent variables are the pillar diameter D_0 and the pitch distance in x-direction D_x. However, we also tested the different structural pillar periodicities ($N_p = 3, 4, 5, 10$) in different simulations.

References

1. Heller, M. & Bruus, H. A theoretical analysis of the resolution due to diffusion and size dispersion of particles in deterministic lateral displacement devices. *J. Micromech. Microeng.* **18,** 075030–7 (2008).
2. Long, B. R. *et al.* Multidirectional sorting modes in deterministic lateral displacement devices. *Phys Rev E Stat Nonlin Soft Matter Phys* **78,** 046304–9 (2008).
3. Cerbelli, S. Separation of polydisperse particle mixtures by deterministic lateral displacement. The impact of particle diffusivity on separation efficiency. *Asia-Pac. J. Chem. Eng.* **7,** S356–S371 (2012).
4. Kulrattanarak, T. *et al.* Mixed motion in deterministic ratchets due to anisotropic permeability. *Journal of Colloid and Interface Science* **354,** 7–14 (2011).
5. Alshare, A. A., Strykowski, P. J. & Simon, T. W. Modeling of unsteady and steady fluid flow, heat transfer and dispersion in porous media using unit cell scale.

International Journal of Heat and Mass Transfer **53,** 2294–2310 (2010).
6. Cerbelli, S., Giona, M. & Garofalo, F. Quantifying dispersion of finite-sized particles in deterministic lateral displacement microflow separators through Brenner's macrotransport paradigm. *Microfluid Nanofluid* **15,** 431–449 (2013).
7. Vernekar, R., Krüger, T., Loutherback, K. & Morton, K. Anisotropic permeability in deterministic lateral displacement arrays. *arXiv.org* (2016).
8. Inglis, D. W. Efficient microfluidic particle separation arrays. *Appl. Phys. Lett.* **94,** 013510–4 (2009).
9. Frechette, J. & Drazer, G. Directional locking and deterministic separation in periodic arrays. *Journal of Fluid Mechanics* **627,** 379–23 (2009).